# Supporting information

# Miniaturized Sensing Probes Based on Metallic Dielectric Crystals Self-assembled on Optical Fiber Tips

Marco Pisco [a,†], Francesco Galeotti [b,†], Giuseppe Quero [a], Agostino Iadicicco [c], Michele Giordano [d,*], Andrea Cusano [a,*]

[a] Optoelectronic Division - Engineering Department, University of Sannio, Benevento, Italy

[b] Institute for Macromolecular Studies, National Research Council, Milano, Italy

[c] Department of Engineering, University of Naples "Parthenope", Naples, Italy

[d] Institute of Composite Biomedical Materials, National Research Council, Naples, Italy.

* Address correspondence to: a.cusano@unisannio.it; gmichele@unina.it

† M. Pisco e F. Galeotti contributed equally to this work

## 1. Variation of lattice period with casting procedure

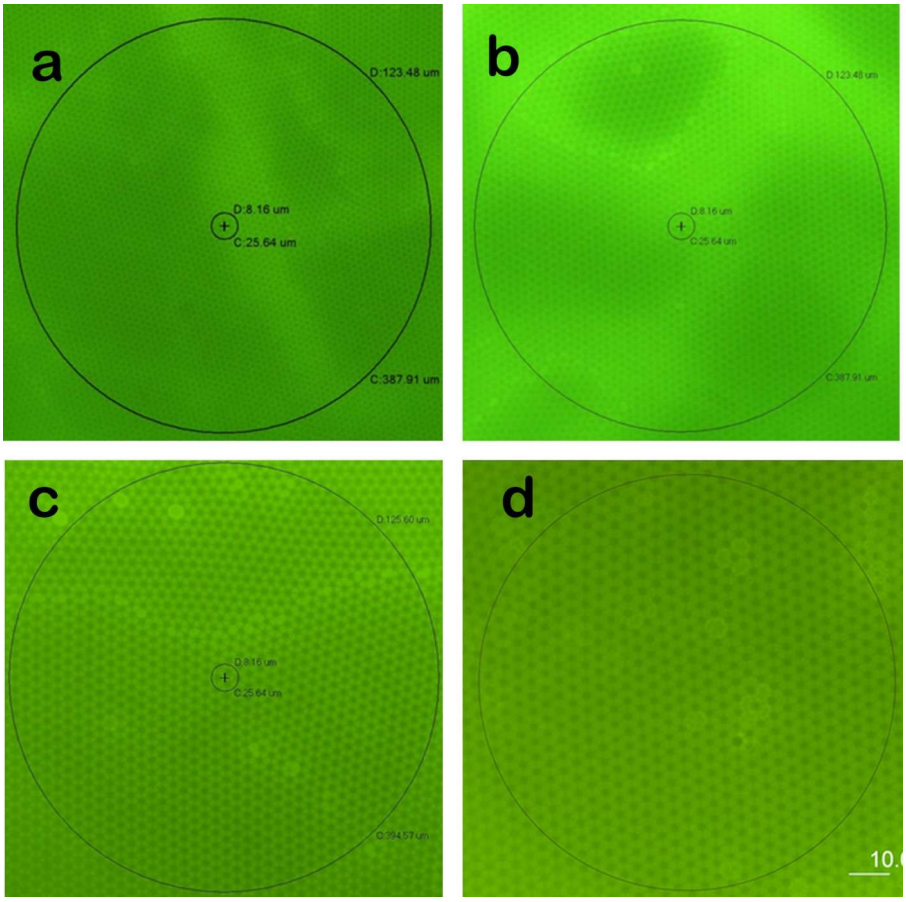


**Figure S1.** Fluorescence microscopy images of honeycomb patterns with different lattice periods (a) : 1.7 µm, b) : 2.5 µm, c) : 3.2 µm, d) : 3.9 µm) prepared on the fiber by varying the casting procedure. The black circle of 125 µm of diameter has been traced to indicate the position of the fiber facet.

## 2. Evaluation of the degree of order

For quantitative analysis, the degree of order of the pattern fabricated on the optical fiber facet can be evaluated using Voronoi polygon analysis.[1] A Voronoi polygon is the smallest convex polygon surrounding a point whose sides are perpendicular bisectors of the lines between a point and its neighbors. The Voronoi construction analysis considers the coordination number, n, of a polygon, which is the number of sides of a Voronoi polygon, and $P_n$, which is the fraction of the number of polygons that have coordination number n. Based on this analysis, the conformation entropy can be calculated using the following formula:

$$S=-P_n \sum \ln P_n$$

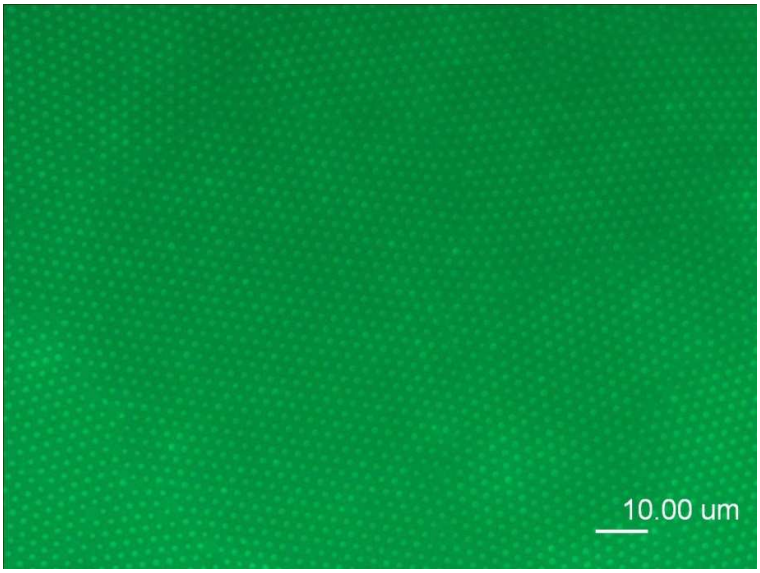


**Figure S2.** Fluorescence microscopy view of the central area of the patterned optical fiber tip (sample 1).

To perform this calculation, we extrapolated the maxima from the fluorescence microscopy image shown in Figure S2 using ImageJ software.[2] This image can be taken as a representative example of the packing obtainable by applying the breath figure procedure on the optical fiber under the conditions described in the main article. By considering only the portion of film that corresponds to the fiber tip, we obtained the image in Figure S3. By applying to this image the Voronoi tessellation, the diagram shown in Figure S4 is obtained.

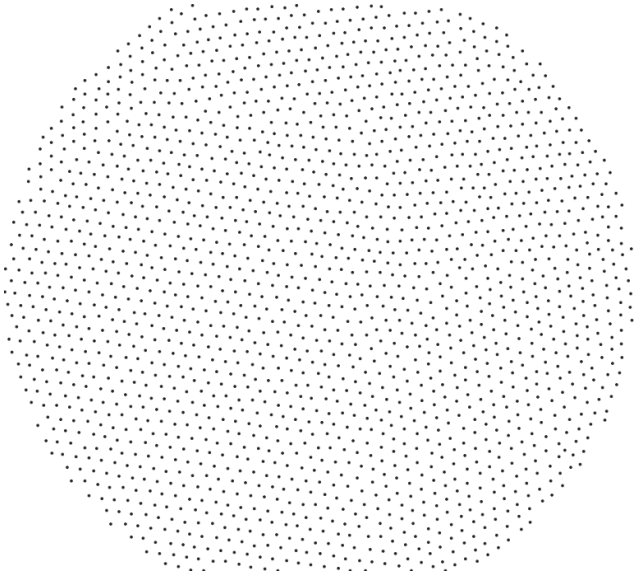

**Figure S3.** Extrapolated maxima image of sample 1.

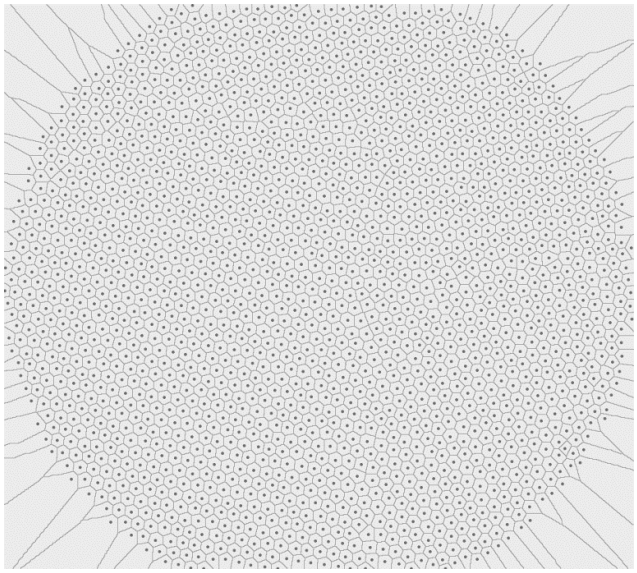

**Figure S4.** Voronoi diagram of sample 1.

We calculated that the probabilities of polygons with four, five, six and seven nearest neighbors ($P_4$, P5, $P_6$, and $P_7$) are 0.0005, 0.03, 0.97 and 0.0005, respectively (the external boundary points were excluded from the calculation). This corresponds to a conformal entropy of 0.15.
Because S=0 in perfect hexagonal packing and S=1.71 in random packing, we can evaluate our structures as being very close to perfect hexagonal packing with a small number of defects.

(1) Limaye, A. V.; Narhe, R. D.; Dhote, A. M.; Ogale, S. B. Evidence for Convective Effects in Breath Figure Formation on Volatile Fluid Surfaces *Phys. Rev. Lett.* **1996**, *76*, 3762–3765.

(2) Schneider, C. A.; Rasband, W. S.; Eliceiri, K. W. NIH Image to *ImageJ*: 25 years of image analysis *Nat. Meth.* **2012**, *9*, 671–675.

## 3. Numerical analysis

*Numerical results obtained with the unit cell based model*

The simulations were carried out using the finite-element method (FEM) with the commercial modeling tool COMSOL Multiphysics® - RF Module (COMSOL Inc., Burlington MA, USA).

To numerically retrieve the reflectance of the photonic crystals using FEM, a common approach requires the calculation of the scattering parameters of a slab that consists of the unit cell with periodic boundary conditions.[47-49]

Rather than considering an (honeycomb) primitive unit cell replicated by the Blok periodic boundary conditions, we selected a non-primitive rectangular cell composed of hexagonal tiling (see Figure S5), and to reduce the computation burden, we restricted the computational domain to one quarter of this rectangular cell. On the bottom of the slab, we assumed a homogenous glass substrate (the optical fiber), while on the top, we used air (the surrounding medium).

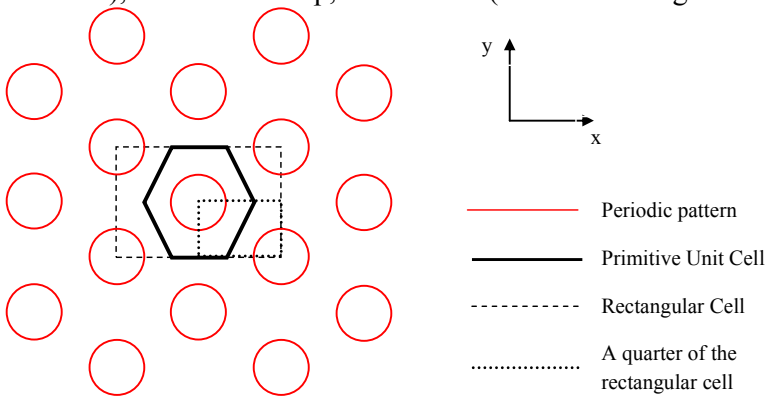


**Figure S5**. Schematic of the periodic hexagonal pattern. The primitive unit cell is a hexagon. The dotted lines indicate the selected rectangular (non-primitive) cell and the corresponding quarter cell used in the simulations.

By exploiting the crystal symmetry, one quarter of cell was transversely terminated with two horizontal, perfectly electric-conducting and two vertical, perfectly magnetic-conducting walls to simulate a normally incident plane-wave with a vertically polarized electric field.[47-48] The input power was set to 1 W. The structural parameters used for the simulations were determined from the morphological characterizations. For the sample 1, the dimensional parameters used for the simulation are hole diameters of 0.95 μm, pitch of 2.67 μm, hole depths of 1.78 μm, base layer height of 0.72 μm and gold thickness of 33 nm. The refractive index of glass and polystyrene were 1.45 and 1.58, respectively. Both losses and the dispersion of gold were taken into account.[23]

On the bottom of the slab, we assumed a homogenous glass substrate (playing the role of the optical fiber substrate), while above we placed an air layer (acting as the surrounding medium).

In Figure S6, the numerical reflectance spectrum (blue line) is reported and compared with the experimental results (black line) obtained in the wavelength range 1250-1650 nm.

From the reported data, it can be noted that the numerical and experimental data are consistent and agree well, even if two main differences can be easily observed. The first is related to the reflectance values. Maximum reflectances of 25% and 50% were found for the experimental and numerical data, respectively. This mismatch can be explained considering the unavoidable fabrication defects with respect to the ideal structure considered in the numerical analysis. The second difference pertains to the presence of narrow peaks and dips superimposed on the broadband reflectance peak in the numerical spectrum, such as those located at 1260 nm, 1330 nm and 1392 nm.

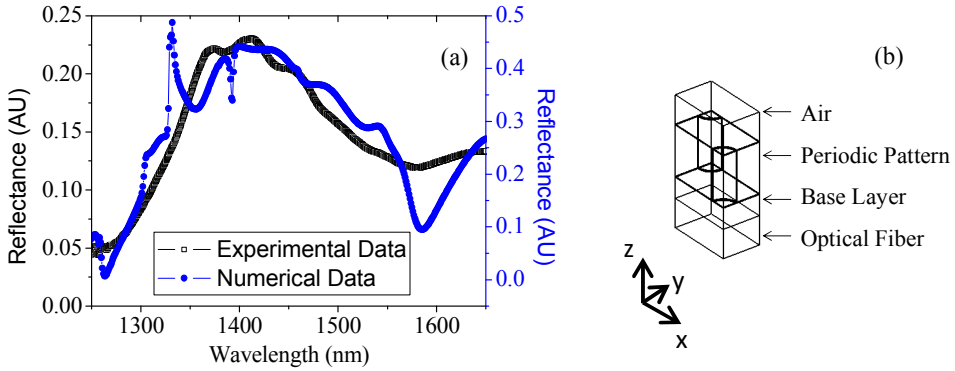


**Figure S6**. (a) Experimental reflectance spectrum in comparison with the numerical reflectance retrieved by the unit cell based model; (b) Computational domain for the unit cell based model

To determine the nature of these peaks, we carefully examined the electric field distributions and the associated losses in the metallic and dielectric domains. Specifically, to highlight the presence of surface plasmons in the conformal metal layer, we show in Figure S7 the integral of the time-averaged "resistive heating" over the metallic subdomains versus wavelength (see the Methods section for resistive heating analytical formula). Resistive heating $q$ is defined as the scalar product between the current density, $j$, and the electric field vector, $e$, so the time-averaged resistive heating can be expressed as $Qav = \langle q \rangle = \langle j \cdot e \rangle$.

More specifically, using the time average theorem, we calculated the time-averaged resistive heating as a function of the current density and electric field in the phasor domain as

$$Qav = \frac{1}{2}\mathrm{Re}\{J \cdot E^*\} \tag{1}$$

with * designating the complex conjugate; then, from the constitutive equation of the current density ($J = \sigma E$) and from the complex permittivity $\varepsilon = \varepsilon' - j\varepsilon'' = \varepsilon' - j\frac{\sigma}{\omega}$, we obtain the time-averaged resistive heating in the form

$$Qav = \frac{1}{2}\mathrm{Re}\{\sigma E \cdot E^*\} = \frac{1}{2}\omega\varepsilon''|E|^2 \tag{2}$$

where $\sigma$ is the conductivity and $\omega$ is the angular frequency.

The integral of the time averaged resistive heating represents the ohmic losses due to surface plasmon excitation. These losses, often considered an undesired effect because they limit the performance of the plasmonic based devices,[1] are used here as an indicator of the presence of surface plasmons.

In our analysis, we found that the resistive heating losses were always present and almost constant over the entire wavelength range investigated, but they rapidly increase at 1260 nm, 1330 nm and 1392 nm. In the inset of Figure S7, we show the normalized electric field distributions along two orthogonal slices in the xz and yz planes (centered in the computational domain) at wavelengths of 1260 nm, 1330 nm, 1392 nm and 1450 nm. The field distributions at 1260 nm, 1330 nm and 1392 nm are indicated by specific field distributions within the patterned structure that clearly resemble guided resonances modes in a periodic pattern. The field distribution at 1450 nm is shown because it is representative of the field distribution over the entire wavelength range. The sharp spectral features can be definitively attributed to the presence of specific hybrid surface plasmonic-photonic resonances, which arise from the periodic metal-dielectric pattern but are not visible in the experimental spectra. The mismatch may be explained by taking into account the Gaussian shape of

the fundamental mode propagating in the core of a single-mode optical fiber and the limited patterned area illuminated in the optical fiber tip.

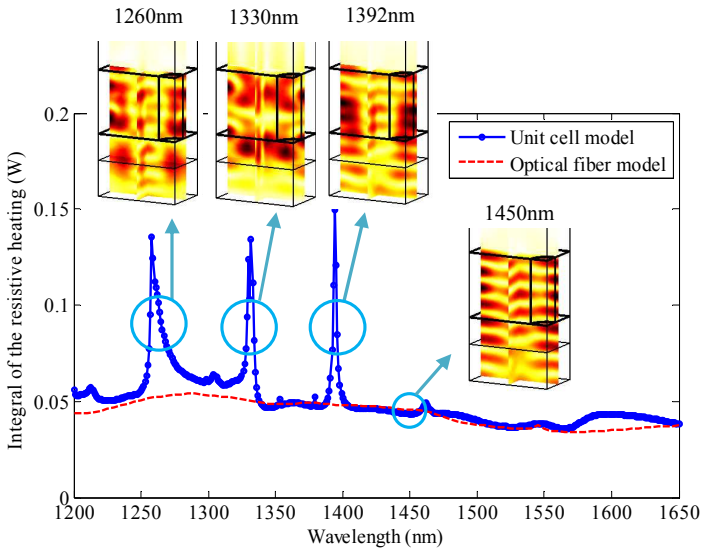


**Figure S7.** Integral of the resistive heating over the thin conformal gold layer for sample 1 calculated using the unit cell model and with the optical fiber model. Inset: Normalized electric field distributions (unit cell model) along two orthogonal slices in the xz and yz planes at different wavelengths

To improve the predictive capability of our analysis, we developed a novel numerical model that considers a Gaussian-like mode as the input light and takes into account the finite size of the periodic structure, including a limited number of unit cells. The numerical results are reported in the main text. Here, for completeness, the integral of the resistive heating over the thin conformal gold layer for sample 1 is also reported.

(1) Coppens, Z. J.; Li, W.; Walker, D. G.; Valentine, J. G. Probing and Controlling Photothermal Heat Generation in Plasmonic Nanostructures. *Nano Lett* **2013**, *13*, 1023-1028.

## 4. Experimental setup for spectral characterizations.

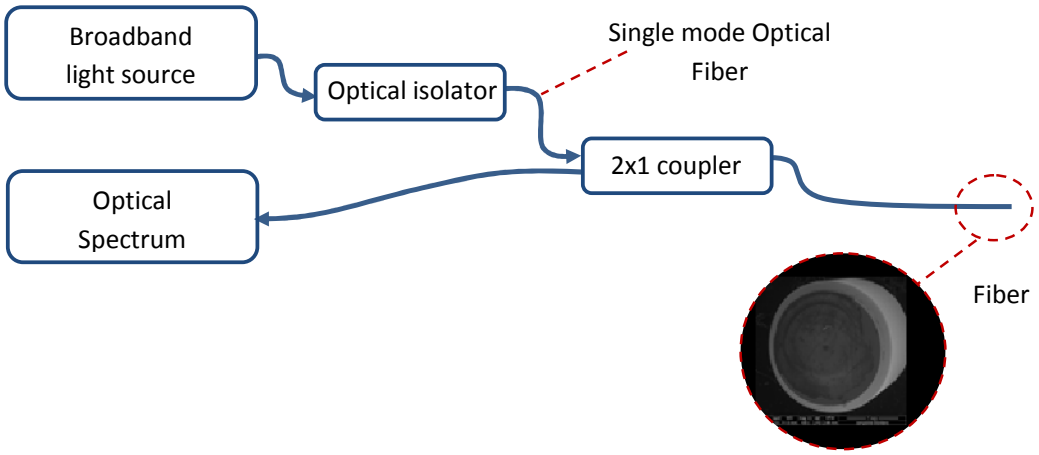


**Figure S8.** Schematic of the experimental setup used for the reflectance spectra characterization.

## 5. Temperature cross-sensitivity

In Fig. S9 we report the resonant wavelength variation of a sample, coated with 35nm thick conformal layer of gold, as a function of the environment temperature. Measurements have been carried out by inserting the fiber tip device in a properly realized thermostated chamber. A temperature sensitivity as low as approximately 7pm/°C was obtained.

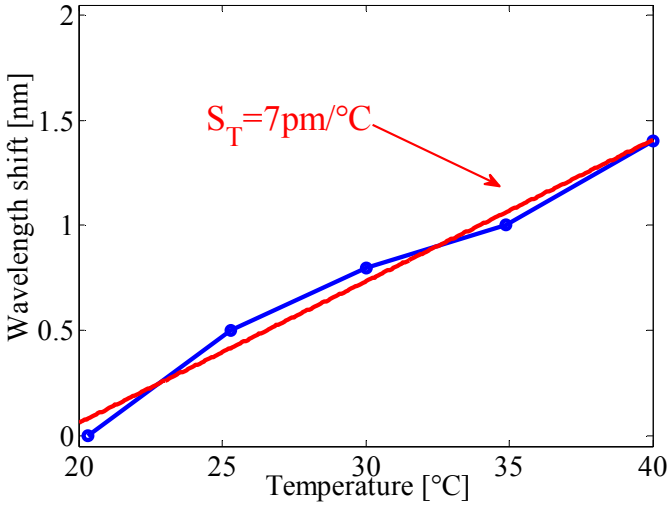


**Figure S9** Wavelength shift versus temperature

## 6. Trends for device design

The proposed optical platform, constituted of a hexagonal metallo dielectric pattern on the optical fiber tip, offers intrinsically high degrees of freedom in its design.

In order to elucidate the relation between the optical reflectance and the geometrical parameters of the structures under investigation, in figure S10, we report the results of few numerical simulations aimed to illustrate the combined effects of the array periodicity, the hole diameter and structure height on the reflectance. For the numerical simulations, we used the optical fiber model introduced in the main text.

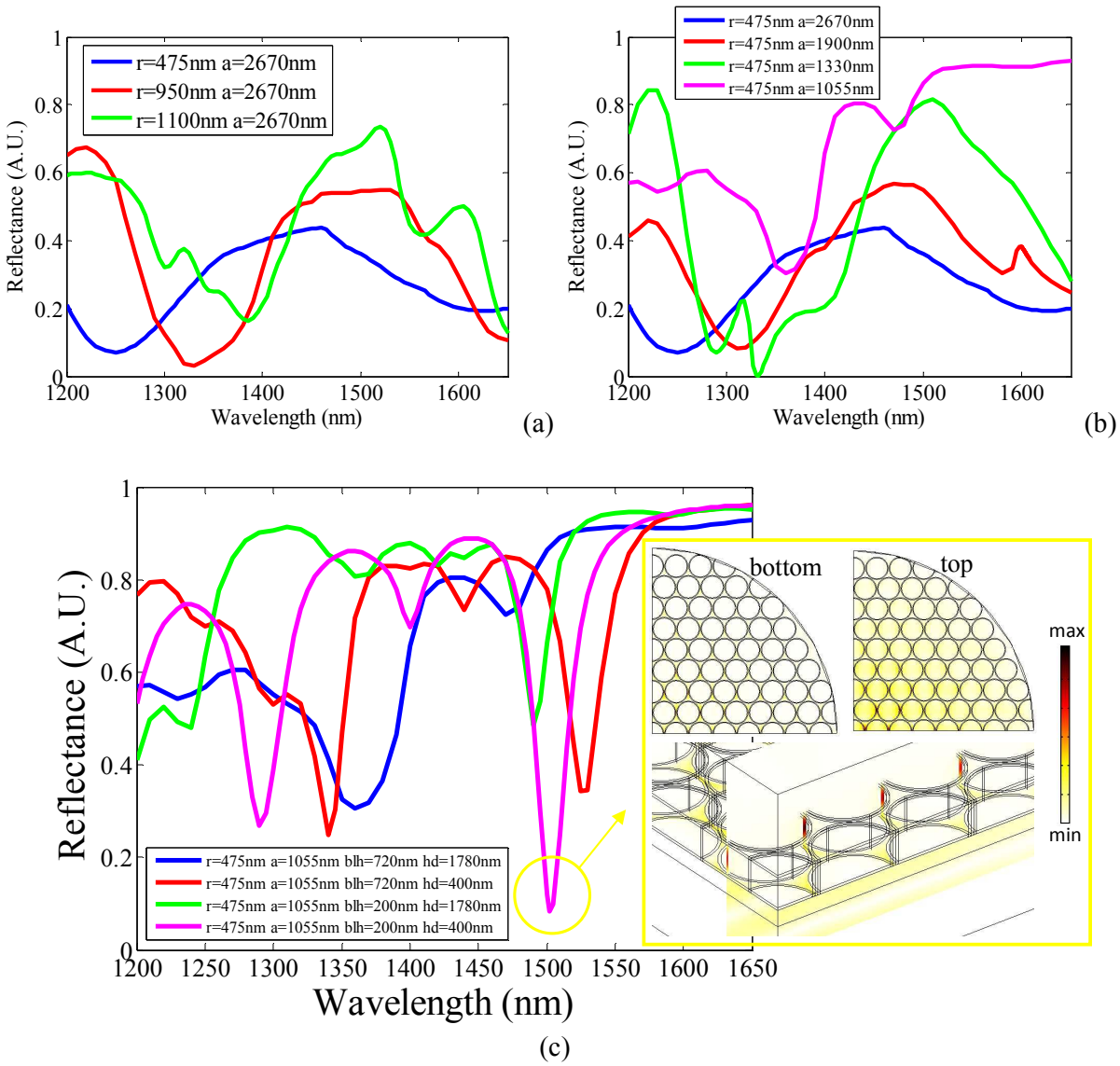


**Figure S10** Numerical reflectance retrieved by the optical fiber based model for a hexagonal metallo dielectric periodic structure on the optical fiber tip with (a) different values of the holes radius "*r*" (b) different values of the holes period "*a*" (c) different values of the hole depths "*hd*" and base layer height "*blh*" respectively. Inset: Normalized electric field distribution at 1505nm in a slice at the bottom (gold disks) and at the top (holes in metal film) of the metal dielectric structure. Below the lateral view of the normalized electric field distribution.

In figure S10a, we show the numerical reflectance for a hexagonal metallo dielectric periodic structure on the optical fiber tip with different values of the holes radius "r". Specifically, we started from the dimensional parameters used for the simulation of the sample 1: hole diameters of 0.95 μm

(*r=475nm*), pitch a=2.67 μm, hole depths hd=1.78 μm, base layer height blh=0.72 μm and gold thickness of 33 nm. Then we varied the radius up to 1100nm.

Similarly, in figure S10b, we show the numerical reflectance of the periodic metallo dielectric structure with different values of the holes period "a". We started from the dimensional parameters of the sample 1 and then we decreased the period down to 1055nm.

In both cases, by increasing the ratio r/a, the mean reflectance increases and the presence of further resonances can be seen (i.e. see the dip at the wavelength around 1560nm for r=1100nm and a=2670nm or the dip at the wavelength around 1360nm for r=475nm and a=1055nm).

Finally, in figure S10c, we show the numerical reflectance for different values of the hole depths "hd" and base layer height "blh", respectively. We started from the reflectance reported in figure S10b featured by two weak resonances around 1360nm and 1480nm, obtained with the following dimensional parameters: r=475nm a=1055nm blh=720nm hd=1780nm. By retaining the same pattern, we reduced the hole depth and the base layer height down to 400nm and 200nm respectively. The numerical analysis results suggest that the holes depth and base layer height can be judiciously used to tune the resonance wavelengths and to improve the sharpness of the spectral features. Sharper resonances have been obtained indeed by promoting a stronger mutual interaction among the electric field distributions associated to the gold disks (at the bottom) and the holes (at the top) of the metallo dielectric structure.

Overall, the geometrical parameters of the proposed optical platform can be used to improve and to tailor the reflectance spectral features for a specific application.